Korea-Australia Rheology Journal
Vol. 16, No. 1, March 2004 pp. 17-26

Microstructure and shear modulus in concentrated dispersions of bidisperse charged spherical colloids

Myung-Suk Chun*, Sangwoo Lee, Tae Seok Lee and Jae Seol Cho
Complex Fluids Research Team, Korea Institute of Science and Technology (KIST), PO Box 131, Cheongryang, Seoul 130-650, South KOREA

(Received December 27, 2003)

Abstract

We examine rigorous computations on microstructural as well as rheological properties of concentrated dispersions of bidisperse colloids. The NVT Monte Carlo simulation is applied to obtain the radial distribution function for the concentrated system. The long-range electrostatic interactions between dissimilar spherical colloids are determined using the singularity method, which provides explicit solutions to the linearized electrostatic field. The increasing trend of osmotic pressure with increasing total particle concentration is reduced as the concentration ratio between large and small particles is increased. From the estimation of total structure factor, we observe the strong correlations developed between dissimilar spheres. As the particle concentration increases at a given ionic strength, the magnitude of the first peak in structure factors increases and also moves to higher wave number values. The increase of electrostatic interaction between same charged particles caused by the Debye screening effect provides an increase in both the osmotic pressure and the shear modulus. The higher volume fraction ratio providing larger interparticle spacing yields decreasing high frequency limit of the shear modulus, due to decreasing the particle interaction energy.

Keywords **:** bidisperse colloid, radial distribution function, osmotic pressure, structure factor, shear modulus, suspension rheology

1. Introduction

Concentrated colloidal suspensions depart from Newtonian behavior. They behave as solids requiring a finite stress, before deforming continuously as a liquid. The qualitative nature of the rheological response is intimately related to the microstructural property, where the colloidal interactions responsible for non-Newtonian or non-Hookean behavior at rest often dominate the response in flows. Mixtures of concentrated colloidal suspensions are of substantial fundamental and practical significance in the processing of complex fluids, such as nano-particle dispersion, biological fluids, and particulate processing (Russel *et al.*, 1989; Wagner and Klein, 1991; Larson, 999).

Since the microstructural analysis of multiparticle interactions is not succinct, most of the relevant studies have been confined to dilute systems. It was reported that the osmotic pressure for a wide concentration range of proteins or other electrostatically stabilized colloids may be calculated accurately *via* use of extended Derjaguin-Landau-Verwey-Overbeek (DLVO) theory (Bowen and Williams, 1996; Bowen *et al.*, 1999). They examined the application of osmotic pressure in the calculation of the gradient diffusion coefficient from the general Stokes-Einstein equation, where their model takes into account multiparticle electrostatic interactions with the nonlinear Poisson-Boltzmann (P-B) field, London-van der Waals forces, and the entropic pressure. Later, they compared the particle concentration dependency upon the thermodynamic coefficients determined by dilute limit, hypernetted-chain closure, radial distribution method, and cell model calculation (Bowen *et al.*, 2000).

The monodisperse colloidal suspension is a well-established model for theoretical investigations. However, this ideal system is hardly found in practical situations. The distribution of particle size explicitly affects the microstructure of colloidal dispersions, and this behavior becomes more significant with an increase of the particle concentration as shown in Fig. 1. The difficulty of the relevant analytical solution will be dramatically increased, even though it is a bidisperse problem, i.e., bimodal mixtures of species with different sizes or different size distributions.

The microstructural properties of a colloidal dispersion can be studied by Monte Carlo simulations, and they provide an exact answer for the given model within statistical

*Corresponding author: mschun@kist.re.kr

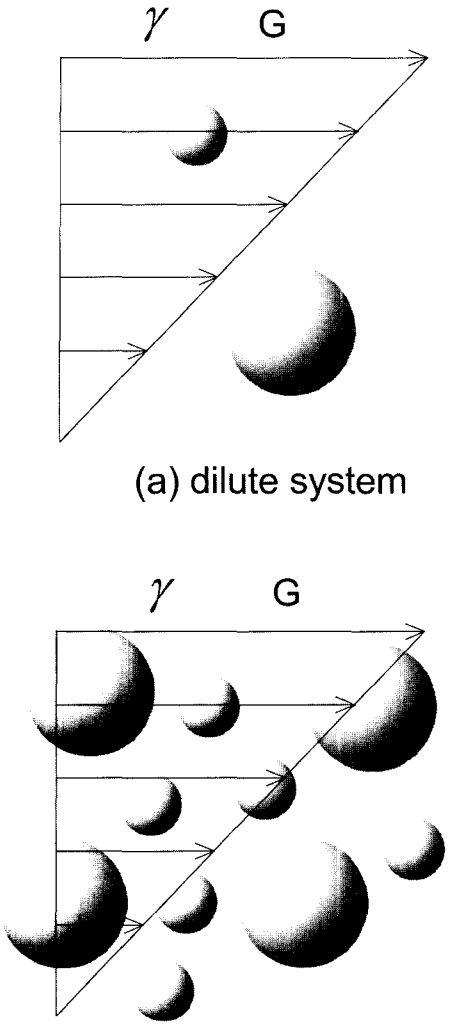

Fig. 1. Schematic of bimodal colloid dispersion in the shear flow.

uncertainty. Very recently, Chun and Bowen (2004) successfully determined the radial distribution function by employing the Monte Carlo simulation for bidisperse charged colloids with higher concentration. In order to recognize the usefulness of their study, simulation results were compared with results from theoretical work obtained using an integral equation method. In their investigation, the rigorous calculation of the long-range electrostatic interaction with the linearized P-B field was performed using a singularity method, which was originally proposed by Phillips (1995) as a useful scheme for multisphere systems. This method is similar to that described by Dabros (1985) for use in low-Reynolds-number hydrodynamics problem.

In this study, we obtain the radial distribution function for bidisperse colloidal suspension performing the Metropolis Monte Carlo simulation. The long-range force due to the electrostatic repulsion between dissimilar spheres is considered, although the colloidal interactions originate from various forces. For example, the van der Waals dispersion forces between two dissimilar approaching spheres act over a relatively long range. Utilizing the radial distribution function, both the osmotic pressure and static structure factor are estimated for suspensions of both uncharged and charged cases. The shear modulus is an important physical property of viscoelastic materials. From the estimation of shear modulus, its concentration dependency is investigated as a function of the volume fraction ratio of large to small spheres and we discuss the encountered phenomena.

2. Radial distribution function and microstructure of concentrated dispersion

2.1. Osmotic pressure from Monte Carlo simulations

We start with the osmotic pressure of a colloidal suspension which provides a quantification of the interactions between colloids in a concentrated system. The osmotic pressure Π is related to the thermodynamic coefficient S as follows (Bowen *et al.*, 2000)

$$S(C) = \frac{3kT}{4\pi a^3}\left[\frac{\partial \Pi(C)}{\partial C}\right]^{-1} \tag{1}$$

where C is the particle concentration in terms of volume fraction, kT the Boltzmann thermal energy, and a the sphere radius. Note that the coefficient $S(C)$ coincides with the structure factor of the suspension at the zero scattering vector. The osmotic pressure is expressed in the form of virial equation as (Bowen and Williams, 1996)

$$\Pi(C) = \frac{3kT}{4\pi a^3} C(1 + A_2 C + A_3 C^2 + \ldots) \tag{2}$$

where A_2 and A_3 are osmotic virial coefficients. It is possible to derive the analytical solution in power series of the particle concentration as

$$S(C) = 1 - 2A_2 C + (2A_2^2 - 3A_3)C^2 + O(C^3). \tag{3}$$

With the radial distribution function $g(s)$, A_2 is represented by

$$A_2 = \frac{3}{2a^3}\int_0^\infty [1 - g(s)]s^2 ds. \tag{4}$$

For the center-to-center separation distance s, the surface-to-surface distance s' corresponds to $s - (a_l + a_s)$ for dissimilar spheres, whereas s' equals to s-$2a_l$ for two large spheres and s-$2a_s$ for two small spheres.

Many investigations exist for the analysis on the radial distribution function. For a dilute suspension, the radial distribution function is simply given by the Boltzmann distribution (Chun and Bowen, 2004)

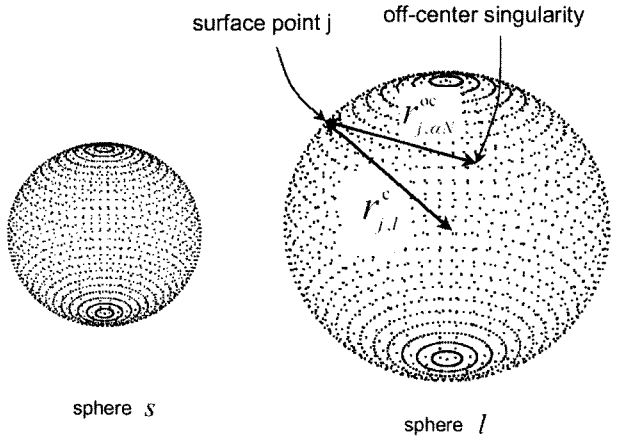

Fig. 2. Pair interaction between two charged spherical colloids l (large) and s (small) of radii a_l and a_s, where surface points spaced at $\pi/32$ rads in θ and φ directions are shown on particles for estimation of electrostatic potential.

$$g(s) = \exp\left(-\frac{E(s)}{kT}\right). \tag{5}$$

Here, $E(s)$ is the pairwise interaction energy between spheres (e.g., large-large, large-small, small-small) separated by a distance s. We represent $E(s)$ of uncharged hard spheres by a Lennard-Jones 6:12 potential. For charged spheres as shown in Fig. 2, $E(s)$ is obtained applying the singularity method presented in Appendix A.

Once the effect of long-range colloidal interactions is absent in the concentrated suspension, the radial distribution function can be computed by integral equations, perturbation methods, and Monte Carlo simulations (Russel *et al.*, 1989). Among these, the Monte Carlo simulations enable the prediction of the charged suspension over the full range of particle concentrations.

2.2. Static structure factor

The important microstructural information can be acquired by means of the structure factor that gives all length scale data (Ottewill *et al.*, 1995; Ottewill, 1996). Considering the phase difference between the scattered beam from two particles at $\boldsymbol{r}_i^l$ and $\boldsymbol{r}_j^s$, the scattering vector $\boldsymbol{Q}$ has a magnitude $(4\pi/f)\sin(\theta/2)$, where f is the wavelength in the dispersion medium, and θ the scattering angle. The static structure factor $S_f(\boldsymbol{Q})$ for a bidisperse suspension can be directly obtained from the $g(s)$, defined as

$$S_f(\boldsymbol{Q}) = \frac{1}{N}\sum_{i=1}^{N_l}\sum_{j=1}^{N_s}\langle exp(i\boldsymbol{Q}\cdot(\boldsymbol{r}_i^l - \boldsymbol{r}_j^s))\rangle \tag{6}$$

where N $(= N_l + N_s)$ denotes the number of spheres and the brackets mean an ensemble average. After spherically-averaging, Eq. (6) yields

$$S_f(Q) = \delta_{ls} + \frac{4\pi\sqrt{n_l n_s}}{Q}\int_0^\infty [g(s)-1]s\sin Qs\,ds \tag{7}$$

where δ_{ls} is the Kronecker delta function, both n_l and n_s the number densities of each sphere, and Q the wave number. The $g(s)$ for bidisperse suspension, which takes three kinds of particle correlations simultaneously, measures the relative density of neighboring spheres at a distance s from a reference sphere. It is known that the Fourier transformation from Q-space (reciprocal space) to real space gives $g(s)$.

3. Shear modulus and high frequency limit

We sketch some of the underlying rheology associated with viscoelastic materials. In a combination of a Newtonian fluid and a Hookean solid, the shear stress tensor under shear rate γ is defined as (Russel *et al.*, 1989)

$$\tau = \eta'(\omega)\gamma\sin\omega t - \frac{G'(\omega)}{\omega}\gamma\cos\omega t. \tag{8}$$

Here, $\eta'(\omega)$ and $G'(\omega)$ are the dynamic viscosity and the shear modulus, respectively, which are varying periodically in time t with the frequency ω The first term of the viscous response is in phase with the velocity gradient, while the second term of the elastic response is in phase with the strain but 90° out of phase with the velocity gradient. For viscoelastic fluids, mechanical analogs provide the followings

$$\frac{\eta'}{\eta_0} = \frac{1+\frac{\eta'_\infty}{\eta_0}(\lambda\omega)^2}{1+(\lambda\omega)^2} \tag{9}$$

$$\frac{G'}{G'_\infty} = \frac{(\lambda\omega)^2}{1+(\lambda\omega)^2} \tag{10}$$

$$\lambda = \frac{\eta_0 - \eta'_\infty}{G'_\infty} \tag{11}$$

where λ is a single relaxation time, G'_∞ $(= \lim_{\omega\to\infty} G')$ the high frequency limit of the shear modulus, η_0 $(= \lim_{\omega\to 0}\eta')$, and η'_∞ $(= \lim_{\omega\to\infty}\eta')$ low and high frequency limits of the dynamic viscosity, respectively.

We analyze the linear viscoelastic response of concentrated dispersions, focusing on the high frequency limit of the shear modulus. The G'_∞ is important to calculate the shear modulus G', since the shear viscosity for complex fluids such as colloidal dispersions at high frequency vanishes and the shear modulus is completely determined by interparticle forces (Wagner and Klein, 1991). The dynamic shear modulus for a high-frequency (or very sudden) disturbance G'_∞ was identified as a function of the radial distribution function $g(s)$, the interaction energy E, and the particle number density n (Zwanzig and Mountain, 1965; Evans and Lips, 1990; Lionberger and Russel, 1994)

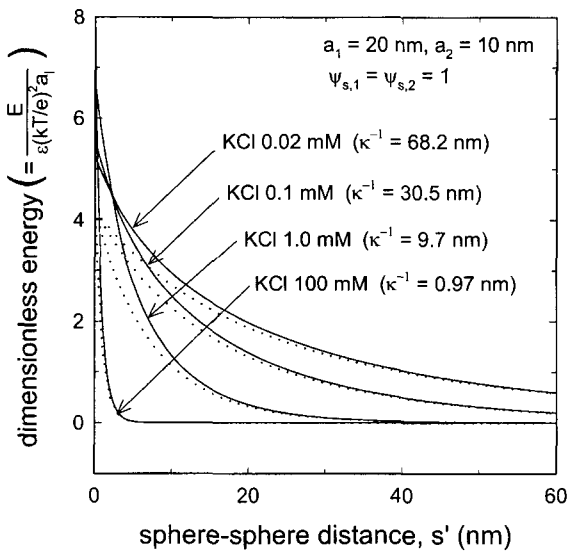

Fig. 3. Dimensionless energy profiles for particle-particle interactions for several inverse Debye lengths with constant surface-charge boundary conditions and a_l = 20 nm and a_s = 10 nm. Dotted curves obtained by analytic approximation correspond to each inverse Debye length.

$$G'_{\infty} = kTn + \frac{2\pi}{15} n^2 \int_0^{\infty} g(s) \frac{d}{ds}\left[s^4 \frac{dE(s)}{ds} \right] ds. \quad (12)$$

Eq. (12) involves two derivatives of $E(s)$, because the first one gives a force, and the second one gives the coefficient of the linear relationship between force and deflection, which is proportional to the modulus.

4. Results and discussion

4.1. Long-range interaction energy

The interaction energy can be computed as addressed in Appendix A. Fig. 3 shows that the interaction energy is changed by the variation of solution ionic strength, where the Debye length κ^{-1} (nm) for aqueous solutions of monovalent electrolytes at 25°C is given by (solution ionic strength (Mol))$^{1/2}$/3.278. The inverse Debye lengths nondimensionalized with sphere 1 (= κa_1) correspond to 0.292, 0.656, 2.06, and 20.6 for ionic strengths of 0.02, 0.1, 1.0, and 100 mMol KCl electrolyte concentration. The electrostatic interaction energy between two dissimilar spheres has an equal dimensionless surface potential of 1. With decreasing solution ionic strength, the interaction energy increases according to the Debye screening effect. We also recognize that the interaction energy increases as the sphere radii ratio (= a_2/a_1) increases. Our results are compared to the analytical approximate results by employing the leading term of the linear superposition with respect to unperturbed potentials, viz, (Ohshima, 1995),

$$E_{EL}^{LSA}(s') = 4\pi a_l a_s \varepsilon \Psi_{s,l} \Psi_{s,s} \frac{\exp(-\kappa s')}{s}. \quad (13)$$

It is obvious that the analytical approximate results become unreliable as two bodies approach more closely.

4.2. Radial distribution function

Once the monodisperse system with hard spheres is treated, the radial distribution functions g are known analytically in the Percus-Yevick approximation (Russel *et al.*, 1989). The Metropolis Monte Carlo simulations sample a canonical ensemble for which the number of particles, temperature, and volume are constant. In this NVT process, the probability governing the random particle displacement is justified as min[1, exp($-\Delta E/kT$)], where $\Delta E = E_{trial} - E_i$ for the i-th step. If the random number is less than this probability, the respective moves are accepted; otherwise the moves are rejected. During the simulations for charged case, the total energies after the particle displacements are evaluated by using a pairwise additive principle with respect to interparticle pair interactions, given as

$$E_{total} = \sum_{j=i+1}^{N_l} \sum_{i=l} E_{l-l}(s) + \sum_{j=i+1}^{N_s} \sum_{i=l} E_{l-s}(s) + \sum_{j=i+1}^{N_s} \sum_{i=l} E_{s-s}(s). \quad (14)$$

We determine the instantaneous interaction energy at arbitrary sphere-sphere separation distances by interpolating with Newton-Gregory forward polynomials of degree 7, where the number of tabulated points for the interpolation ranged from 20 to 28. Interpolating with polynomials was checked by comparing with fitted energy profiles that decay exponentially as functions of the separation distance and the regression coefficients.

In the present study, spheres with a total number of 200 – 400 are introduced in a simulation box. For the particle displacements, the sizes of the random steps in the three coordinate directions are chosen to be 50% of the corresponding dimension of the periodic unit cell. The total volume fraction C equals the addition of volume fractions for large spheres C_l and small spheres C_s. Discarding non-equilibrium configurations and production configurations are taken to be about 2×10^4 and 4×10^4, respectively. For an initial condition, spheres are arranged in face-centered cubic lattices.

We implement a computation of the radial distribution function using a virial expansion based on the integral equation method to compare with Monte Carlo simulation results. Solving the correlation function by the Ornstein-Zernike equation and the Percus-Yevick closure, we can then proceed the particle concentration profile $C(s)$ with the particle concentration in the bulk C, expressed as (Chun and Bowen, 2004)

$$g(s) = \frac{C(s)}{C} = \exp\left(-\frac{E(s)}{kT}\right)(1 + C\, Y_l(s) + \ldots) \quad (15)$$

where the first virial coefficient is defined as

$$Y_l(s) = \int [\exp(-E(s)/(kT)) - 1][\exp(-E(\mathbf{r}, \mathbf{r}_l)/kT) - kT] d\mathbf{r}_1. \quad (16)$$

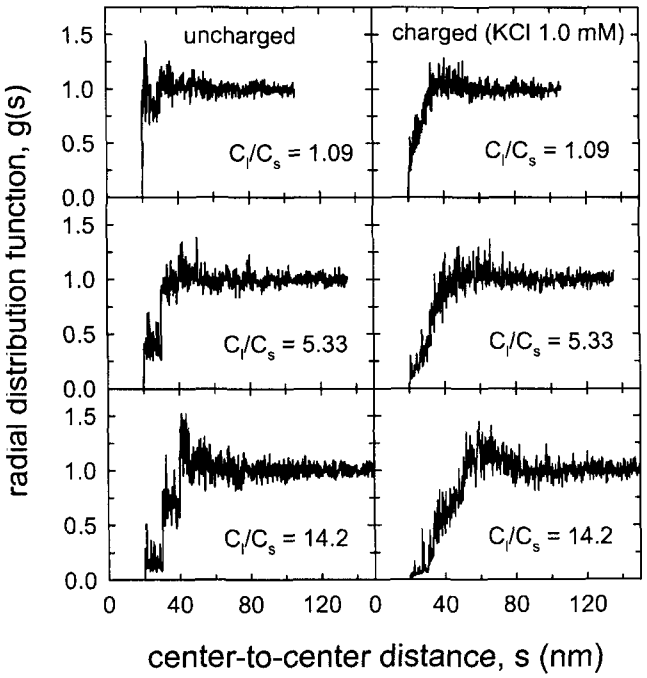

Fig. 4. Mixed radial distribution functions of uncharged as well as charged spheres with $a_l = 20$ nm ($\kappa a_l = 2.06$) and $a_s = 10$ nm ($\kappa a_l = 1.03$) for different volume fraction ratio C_l/C_s at $C = 0.1$.

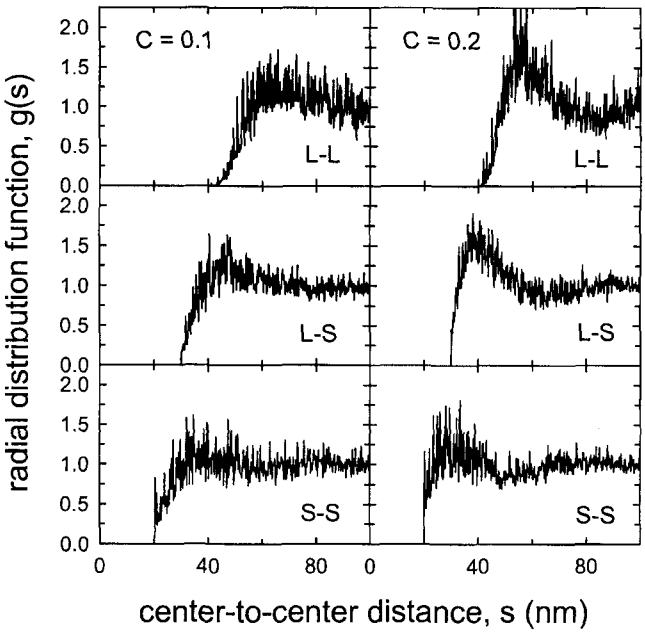

Fig. 5. Independent partial radial distribution functions obtained by dividing each correlation, $a_l = 20$ nm ($\kappa a_l = 2.06$), $a_s = 10$ nm ($\kappa a_s = 1.03$), and $C_l/C_s = 5.33$.

In Eq. (16), one sphere (sphere 1) is at position $\boldsymbol{r}$, a distance s from a second sphere, and a third sphere is at position $\boldsymbol{r}_1$. The integral is over all space around one sphere, and the Mayer function $\exp(-E(\boldsymbol{r}, \boldsymbol{r}_1)/kT) - 1$ depends on the sphere-sphere interaction. The Y_1 is defined in terms of configuration-space integrals that involve interactions both between sphere 1 and 2 and between sphere 1 and 3. Each individual $g(s)$ is estimated for all cases, in which three spheres are alternately assigned with possible combinations of large and small ones. Overall $g(s)$ can be obtained by weighting the individual $g(s)$ with corresponding possibility of choosing. For the case of monodisperse system, it is known that only the first-order effect of C can be reasonably considered without great loss of accuracy (Glandt, 1981). Chun and Bowen (2004) provided that a fairly agreement between the radial distribution function from Monte Carlo simulations and corresponding predictions from the virial expansions is shown at the lower particle concentration with the lower C_l/C_s. The disagreement is developed, however, once the particle concentration increases at lower C_l/C_s or the C_l/C_s increases at lower particle concentration.

Fig. 4 shows the mixed radial distribution function $g(s)$ for a bidispserse suspension of hard spheres with different volume fraction ratio C_l/C_s at the total volume fraction of 0.1. As the volume fraction ratio increases, the $g(s)$ profile has the splitting shape at the distance positions of 20, 30, and 40 nm for the interactions of small-small, small-large, and large-large spheres. The $g(s)$ of charged spheres with equal surface potential is also provided. We point out that, compared to the case of uncharged spheres, the repulsive interactions evidently decrease the density near the sphere. As shown in Fig. 5, it is possible to obtain the partial $g(s)$, i.e., individual $g(s)$ for large-large, large-small, and small-small.

4.3. Structure factor and shear modulus

When the particle concentration is zero, the coefficient A_2 of Eq. (4) has a maximum value corresponding to the dilute asymptote A_2, and it decreases with increasing particle concentration. Once the values of A_2 are known, the osmotic pressure can be computed as functions of the particle concentration. Fig. 6 shows that with increasing particle concentration the osmotic pressure has an overall increasing trend. The volume-average radii of bidisperse spheres are determined as 12.25, 15.61, 16.34, and 17.63 nm with respect to the ratios of particle volume fraction of 1.09, 5.33, 7.38, and 14.2. Regardless of uncharged or charged cases, as the volume fraction ratio increases, the osmotic pressure decreases. Evidently, the increase of electrostatic interaction between same charged spheres caused by the Debye screening effect provides an increase in the osmotic pressure compared to the uncharged case. Corresponding results obtained using either the analytic approximation for energy profile or the analytic expression for osmotic pressure are provided in Fig. 6b, to propose the validity of a rigorous calculation of energy profile as well as Monte Carlo simulations for the radial distribution func-

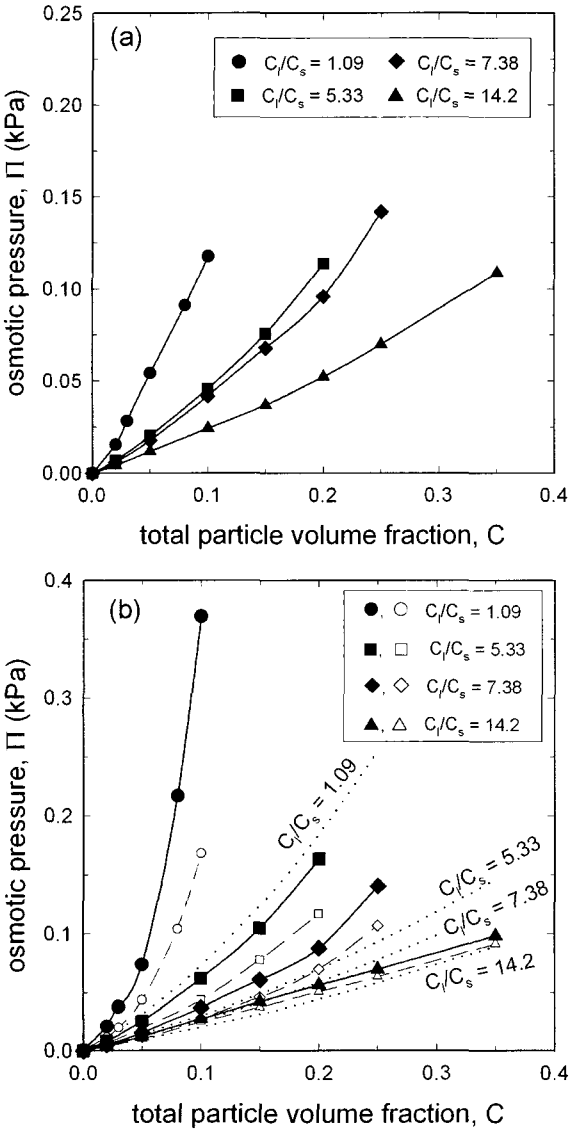

Fig. 6. The plots of the osmotic pressure Π vs particle concentration with different concentration ratios for (a) uncharged hard spheres and (b) charged spheres with $\kappa a_l = 2.06$ and $\kappa a_s = 1.03$. Open symbols correspond to the Monte Carlo results obtained using the analytical energy profile, and dotted lines are determined using A_2 coefficients for the dilute limit case.

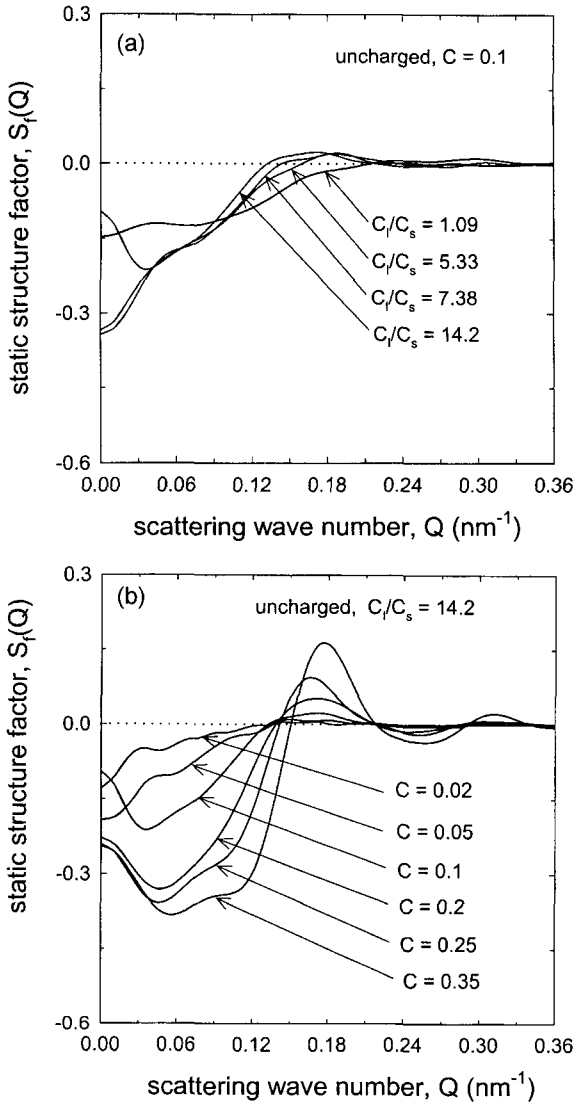

Fig. 7. Static structure factor $S_l(Q)$ of uncharged hard spheres for (a) different volume fraction ratios and (b) different total volume fractions, where a_l = 20 nm, a_s = 10 nm, and λ = 35 nm.

tion. The hypothetical results obtained from the dilute asymptote A_2 show a great deviation. In Fig. 6b, the osmotic pressure obtained using the rigorous energy profile of this study is estimated more than twice that obtained using the analytical energy profile. But, the discrepancy between the two results on the volume fraction change is decreased as the composition of the bimodal suspension becomes disparate.

Figs. 7 and 8 indicate that a structure is built up which depends both on the particle volume ratio and the solution ionic strength. The structure factor in this study ensures the total contributions consisting three kinds of particle correlations (i.e., large-large, large-small, small-small). The strong correlations develop between the two different-sized spheres, and one would expect that the small spheres would tend to fit into the spaces between the larger ones. This is indicated by the increase in magnitude of the first peak in $S_l(Q)$ and its decrease at low Q values as the volume fraction increases at a given ionic strength. The first peak also moves to higher Q values as the volume fraction increases. Compared between uncharged and charged cases, it can be observed that with increase in ionic strength at constant volume fraction a broadening of the peak occurs, which indicates a decrease in strength of the interparticle interaction and a greater motion of the spheres.

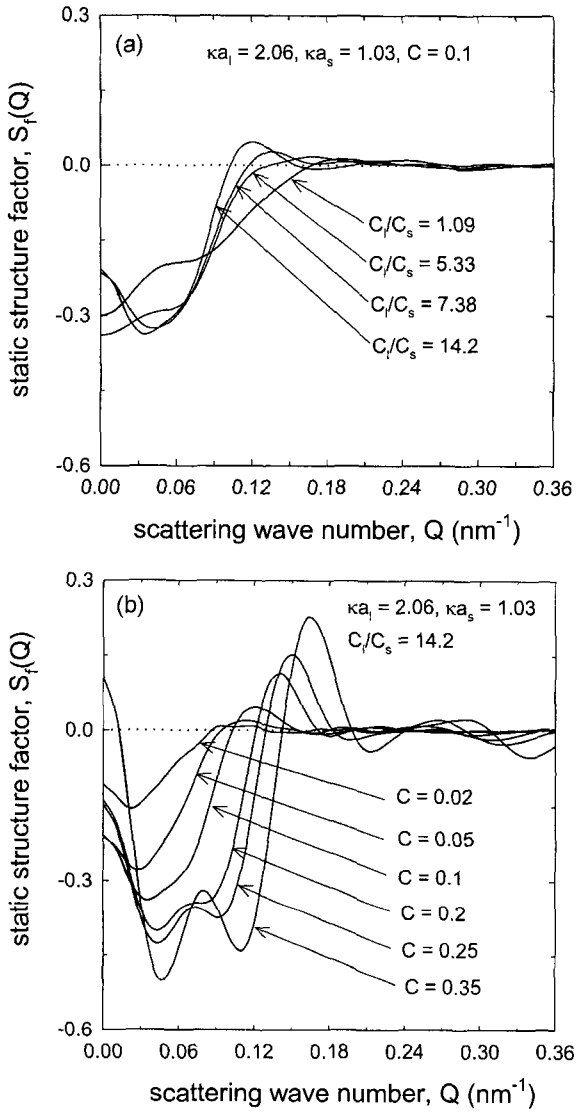

Fig. 8. Static structure factor $S_f(Q)$ of charged spheres for (a) different volume fraction ratios and (b) different total volume fractions, where $a_l = 20$ nm ($\kappa a_l = 2.06$), $a_s = 10$ nm ($\kappa a_s = 1.03$), and $\lambda = 35$ nm.

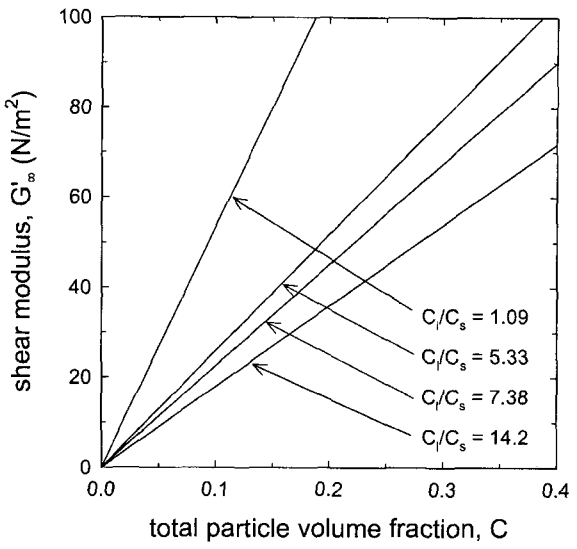

Fig. 9. The plots of the shear modulus G'_∞ vs particle concentration with different concentration ratios for uncharged hard spheres with $a_l = 20$ nm and $a_s = 10$ nm.

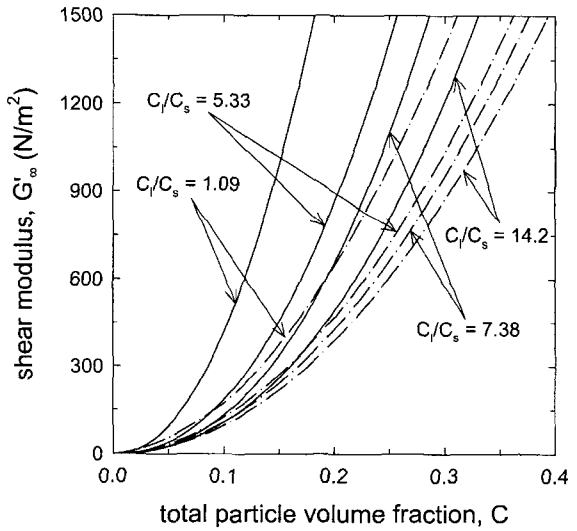

Fig. 10. The plots of the shear modulus G'_∞ vs particle concentration with different concentration ratios for charged spheres with $\kappa a_l = 2.06$ and $\kappa a_s = 1.03$. Dash-dotted curves correspond to the Monte Carlo results obtained using the analytical energy profile.

The shear modulus in colloidal dispersions means how a material deforms under given shear stress. For high frequency oscillations, the shear modulus is closely related to the microstructure. The shear modulus is estimated by ensuring simultaneously mixed contributions of all correations, in which we use the pair interaction energy profiles determined by each volume average radius with respect to each volume fraction ratio. In Fig. 9, the uncharged suspension shows a linear relationship between the particle volume fraction and the shear modulus. In Eq. (12), the first term represents the osmotic pressure, and the second term is pertinent to the effect of particle interaction. In the Lennard-Jones potential for uncharged hard spheres, we determine the relevant coefficients by comparing to the energy curve of sufficiently high concentration of KCl (i.e., 1.0 Mol). The second term of Eq. (12) becomes truly negligible in the case of uncharged suspension.

The shear modulus at each particle volume fraction increases with decreasing ionic strength, as shown in Fig. 10. With increasing particle concentration at KCl 1.0 mMol, the shear modulus increases with the power law exponents in the range 2.1 to 2.3. These values compare well with the previous experimental results obtained on a polystyrene latex (Ottewill, 1996). Regardless of

uncharged or charged cases, as the volume fraction ratio increases, the high frequency limit of the shear modulus G'_∞ is decreased. This is a consequence of changing the number of particles to maintain constant volume fraction, and hence changing the average interparticle spacing. The higher C_l/C_s, which has lower number of particles, exhibits larger interparticle spacing. This is a direct result of decreasing the interaction energy, which yields decreasing G'_∞. As the composition of the bimodal suspension becomes disparate, the suspension has more fluid-like property.

5. Conclusions

Applying Monte Carlo simulations, the singularity method for linearized P-B field, the pairwise additive for many-body interactions, and the linear viscoelastic model, yields quantitative predictions for charged bidisperse suspensions. Our major interest lies in exploring a system of constant particle volume fraction while varying the relative percentage of the two components. The radial distribution function of the colloidal dispersion was obtained for higher particle concentration up to ca. 30 Vol %. The utility of numerical simulations was verified by attempting comparison with analytical approximate results.

It is evident that the effect of electrostatic repulsion due to the Debye screening upon both the osmotic pressure and the shear modulus depends on the particle concentration. As the concentration ratio between large and small particles decreases, both the osmotic pressure and the shear modulus are increased at a given total concentration. This trend can be understood from estimating the static structure factor, in which more small particles tending to fit into the spaces between the larger ones results in the increasing the osmotic pressure. We found that larger interparticle spacing results from the increasing volume fraction ratio, and with increasing charge contribution the colloidal suspension becomes more solid-like. Our computational study provides a framework for applications on the rheology of charged suspensions.

Appendix A: Long-range electrostatic interaction between dissimilar spheres

The singularity method applied in this study has been proved to overcome the restrictions of the Derjaguin approximation as well as the linear superposition approximation. In principle, the electrostatic potential in the liquid can be represented as a sum of contributions from point charges located inside the spheres, if the dielectric constant of solid particle is assumed to be small relative to that of the surrounding liquid. These point charges are expressed by the fundamental singular solution to the linearized P-B equation. The strengths of the singularities are chosen to provide the best possible agreement with the prescribed boundary conditions.

Let us examine a problem of N identical charged spheres interacting in solution. The electrostatic potential is governed by a P-B equation with the linear ansatz

$$\nabla^2\psi = (\kappa a)^2 \sinh\psi \simeq (\kappa a)^2\psi \tag{A1}$$

where the electrostatic potential ψ is normalized by a characteristic surface potential, and the inverse Debye length (or double layer thickness) κ defined as $\sqrt{\left(e^2 N_A \sum_i c_i^o Z_i^2\right)/\varepsilon kT}$ is made dimensionless by the sphere radius a. Note that e is the elementary Coulombic charge, N_A the Avogadro number, ε a dielectric constant, c_i^o the concentration of ion species i far from the sphere (in moles per unit volume), and Z_i its valence. We consider here the condition of overall electroneutrality in an equilibrium solution.

Among boundary conditions known as the constant charge, the constant potential, and the linearized charge regulation, we consider the sphere surfaces S_A having a constant surface-charge density σ, leading to the constant charge boundary condition

$$\boldsymbol{n}\cdot\nabla\psi = \sigma \quad \text{on } S_A \tag{A2}$$

where $\boldsymbol{n}$ is a unit normal vector pointing into the sphere. The singular solution to Eq. (A1) for a point charge at the origin has the form (i.e., $\psi = q\ \exp(-\kappa a r)/r$) with an unknown constant q and the distance r from the origin normalized by the sphere radius. For an isolated sphere suspended in an unbounded solution, the value of q can be determined from the boundary condition.

The bidisperse colloidal suspensions of charged spheres with radii a_l and a_s are considered as shown in Fig. 2, where the subscripts refer to the large and small ones, respectively. Both spheres, when they are not interacting with each other, have surface potentials ψ_s of 1 equal to $kT/e = 25.69$ mV. The principle calculation step is similar to a problem of equal-sized spheres. However, the location of the surface points and the singular points inside the spheres should be newly developed according to the sphere radii ratio a_l/a_s.

The total surface charge outside the spheres is expressed as the addition of the sum of the known contribution of singularities at the sphere centers $\boldsymbol{n}\cdot\nabla\psi_i^{oc}$ and the sum of the corresponding contribution of off-center singularities $\boldsymbol{n}\cdot\nabla\psi_i^{oc}$. There are α off-center singularities for each of the N spheres. Considering the surface charge density σ at a surface point $\boldsymbol{x}_j$, the following is written

$$\sum_{i=l}^{\alpha N} \boldsymbol{n}\cdot\nabla\psi_i^{oc}(\boldsymbol{x}_j) = \sigma(x_j) - \sum_{i=l}^{N} \boldsymbol{n}\cdot\nabla\psi_i^{c}(\boldsymbol{x}_j) \quad \text{for } j = 1 \text{ to } M. \tag{A3}$$

Eq. (A3) provides M linear equations for the αN unknown singularity strengths q_i^{oc}, where M is the total number of surface points of two dissimilar spheres (i.e.,

$N = 2$) and a_l takes the basis of the characteristic length for the sphere radius. Then, the following matrix is formulated.

$$\begin{bmatrix} d_{1,1} & \cdots & d_{1,\alpha} & \cdots & d_{1,2\alpha} \\ \vdots & & \vdots & & \vdots \\ d_{M/2,1} & \cdots & d_{M/2,\alpha} & \cdots & d_{M/2,2\alpha} \\ \vdots & & \vdots & & \vdots \\ d_{M,1} & \cdots & d_{M,\alpha} & \cdots & d_{M,2\alpha} \end{bmatrix} \begin{bmatrix} q_1^{oc} \\ \vdots \\ q_\alpha^{oc} \\ \vdots \\ q_{2\alpha}^{oc} \end{bmatrix} = \begin{bmatrix} b_1 \\ \vdots \\ b_{M/2} \\ \vdots \\ b_M \end{bmatrix} \tag{A4}$$

where

$$d_{j,k} = n \cdot \nabla\left(\frac{\exp(-\kappa a_l r_{j,k}^{oc})}{r_{j,k}^{oc}}\right) \quad \text{for } j = 1 \text{ to } M,\ k = 1 \text{ to } 2\alpha \tag{A5a}$$

$$b_j = \sigma(x_j) - n \cdot \nabla\left(q_1^c \frac{\exp(-\kappa a_l r_{j,1}^c)}{r_{j,1}^c} + q_2^c \frac{\exp(-\kappa a_l r_{j,2}^c)}{r_{j,2}^c}\right). \tag{A5b}$$

From Eq. (A4), the value of q_l^{oc} is found by a least-squares routine that minimizes the sum of squared residuals at the surface points. For surface potential ψ_s, the dimensionless surface charge densities of each sphere are expressed as $\sigma_l = \psi_{s,l}(1 + \kappa a_l)$ and $\sigma_s = \psi_{s,s}\ (1 + \kappa a_s)\ (a_l/a_s)$ for large and small spheres, respectively.

The force on a charged sphere interacting with other charged spheres is calculated by accounting for the spherical coordinates. The strength of each point singularity is determined by satisfying the boundary conditions. Once the solution for the potential is obtained, the force vector $\boldsymbol{F}$ is calculated from the surface integration of normal component of Maxwell stress tensor $\boldsymbol{T}$, as follows

$$F = \int_{S_A} \boldsymbol{T} \cdot \boldsymbol{n} dS_A$$

$$= \int_{S_A} \left[\left(\overline{\Pi} + \varepsilon \frac{\boldsymbol{E} \cdot \boldsymbol{E}}{2}\right)\boldsymbol{I} - \varepsilon \boldsymbol{E}\boldsymbol{E}\right] \cdot \boldsymbol{n} dS_A \tag{A6}$$

where $\boldsymbol{I}$ is the identity tensor and $\boldsymbol{E}(= -\nabla \psi)$ denotes the electric field vector. The electrostatic potential is related to the difference in the local osmotic pressure $\overline{\Pi}$ from the bulk solution given by $\varepsilon\kappa^2\psi^2/2$ (Carnie *et al.*, 1994; Hsu and Liu, 1999). Then the electrostatic interaction energy profile between pairs of spheres with separation distance between two spheres s' can be obtained by integrating the force acting on the sphere,

$$E_{EL}(s') = \int_{-\infty}^{s'} F_x dx = \int_{-\infty}^{s'} \left[\boldsymbol{e}_x \cdot \int_{S_A} \boldsymbol{T} \cdot \boldsymbol{n} dS_A\right] dx$$

$$= \int_{S_A} [\cos\theta T_{rr} - \sin\theta T_{\theta r}] r^2 \sin\theta d\theta d\varphi \tag{A7}$$

where dS_A is defined in spherical coordinates (r, θ, φ).

Nomenclatures

a : particle radius [m]
A_2, A_3 : osmotic virial coefficients [–]
C : particle volume fraction [–]
c_i^o : concentration of ion species i [Mol/m^3]
E : interaction energy [J]
e : elementary charge [Coul]
$\boldsymbol{e}$: unit vector [–]
F : electrostatic force [N]
f : wavelength in the dispersion medium [m]
G' : dynamic shear modulus [N/m^2]
G'_∞ : high frequency limit of the shear modulus [N/m^2]
g : radial distribution function [–]
$\boldsymbol{I}$: identity tensor [–]
k : Boltzmann constant [J/K]
M : total number of surface points [–]
N : number of spheres [–]
N_A : Avogadro number [1/Mol]
$\boldsymbol{n}$: unit normal vector pointing into solvent [–]
n : number density [1/m^3]
$\boldsymbol{Q}$: scattering vector [–]
q : unknown singularity [–]
$\boldsymbol{r}$: position vector [–]
r : distance normalized by sphere radius [–]
S : thermodynamic coefficient [–]
S_A : surface area [m^2]
S_f : static structure factor [–]
s : center-to-center separation distance [m]
s' : surface-to-surface distance [m]
T : absolute temperature [K]
$\boldsymbol{T}$: Maxwell stress tensor [N/m^2]
x : Cartesian coordinate [–]
Y_1 : first virial coefficient in Eq. (16) [m^3]
Z_i : valence of ion species i [–]

Greek Letters

α : number of off-center singularities [–]
γ : shear rate [1/s]
δ : Kronecker delta function [–]
ε : dielectric constant [Coul/V · m]
η_0 : low frequency limit of the dynamic viscosity [kg/m · s]
η' : dynamic shear viscosity [kg/m · s]
η'_∞ : high frequency limit of the dynamic viscosity [kg/m · s]
θ : scattering wave angle [deg]
κ : inverse Debye length [1/m]
λ : relaxation time [s]
$\overline{\Pi}$: difference in local osmotic pressure [N/m^2]
σ : dimensionless surface charge density [–]
τ : shear stress tensor [N/m^2]
ψ : dimensionless potential [–]
ψ_s : dimensionless surface potential of sphere [–]
ω : frequency of oscillation of applied flow [1/s]

<Subscripts>

l	: large
s	: small
p	: particle

<Superscripts>

c	: center
oc	: off-center

Acknowledgements

This work was supported by the International Collaboration Research Fund (M60302000005) from the Korea Ministry of Science and Technology as well as the Basic Research Fund (Grant No. R01-2001-000-00411-0) from the Korea Science and Engineering Foundations (KOSEF) provided to M.-S.C. The authors also thank to Professor W.R. Bowen at the Centre for Complex Fluids Processing of Univ. of Wales, Swansea for valuable discussions on the bimodal colloid system.

References

Bowen, W.R. and P.M. Williams, 1996, The osmotic pressure of electrostatically stabilized colloidal dispersions, *J. Colloid Interface Sci.* **184**, 241-250.

Bowen, W.R., X. Cao and P.M. Williams, 1999, Use and elucidation of biochemical data in the prediction of the membrane separation of biocolloids, *Proceedings of the Royal Society of London Series A - Mathematical, Physical and Engineering Sciences* **455**, 2933-2955.

Bowen, W.R., Y. Liang and P.M. Williams, 2000, Gradient Diffusion Coefficients-Theory and Experiment, *Chem. Eng. Sci.* **55**, 2359-2377.

Carnie, S.L., D.Y.C. Chan and J.G. Gunning, 1994, Electrical Double Layer Interaction between Dissimilar Spherical Colloidal Particles and between a Sphere and a Plate: The Linearized Poisson-Boltzmann Theory, *Langmuir* **10**, 2993-3009.

Chun, M.-S. and W.R. Bowen, 2004, Rigorous Calculations of Linearized Poisson-Boltzmann Interaction between Dissimilar Spherical Colloids and Osmotic Pressure in Concentrated Dispersions, *J. Colloid Interface Sci.* in press.

Dabros, T., 1985, A singularity method for calculating hydrodynamic forces and particle velocities in low Reynolds number flows, *J. Fluid Mechanics* **156**, 1-21.

Evans, I.D. and A. Lips, 1990, Concentration dependence of the linear elastic behavior of model microgel dispersions, *J. Chem. Soc. Faraday Trans.* **86**, 3413-3417.

Glandt, E.D., 1981, Distribution equilibrium between a bulk phase and small pores, *AIChE J.* **27**, 51-59.

Hsu, J.-P. and B.-T. Liu, 1999, Electrical interaction energy between two charged entities in an electrolyte solution, *J. Colloid Interface Sci.* **217**, 219-236.

Larson, R.G., 1999, *The Structure and Rheology of Complex Fluids*, Oxford Univ. Press, New York.

Lionberger, R.A. and W.B. Russel, 1994, High frequency modulus of hard sphere colloids, *J. Rheology* **38**, 1885-1908.

Ohshima, H., 1995, Electrostatic interaction between two dissimilar spheres with constant surface charge density, *J. Colloid Interface Sci.* **170**, 432-439.

Ottewill, R.H., H.J.M. Hanley, A.R. Rennie and G.C. Straty, 1995, Small-angle neutron scattering studies on binary mixtures of charged particles, *Langmuir* **11**, 3757-3765.

Ottewill, R.H., 1996, Application of scattering techniques to polymer colloid dispersions, in *Polymeric Dispersions: Principles and Applications*, (Ed.) Asua, J.M. (229-242), NATO ASI Series E, Kluwer, Boston.

Phillips, R.J., 1995, Calculation of multisphere linearized Poisson-Boltzmann interactions near cylindrical fibers and planar surfaces, *J. Colloid Interface Sci.* **175**, 386-399.

Russel, W.B., D.A. Saville and W.R. Schowalter, 1989, *Colloidal Dispersions*, Cambridge University Press, New York.

Wagner, N.J. and R. Klein, 1991, The rheology and microstructure of charged colloidal suspensions (Leading Contribution), *Colloid Polymer Sci.* **269**, 295-319.

Zwanzig, R. and R.D. Mountain, 1965, High-Frequency Elastic Moduli of Simple Fluids, *J. Chem. Phys.* **43**, 4464-4471.